International Journal of Engineering Research & Technology (IJERT)
ISSN: 2278-0181
Vol. 2 Issue 12, December - 2013

Stabilization and Design of a Hovercraft Intelligent Fuzzy Controller

M. M. El-khatib[1] W. M. Hussein[2]

Military Technical Collage, Cairo, Egypt

ABSTRACT

The hovercraft is a fascinating mechatronic system that possesses the unique ability to float above land or water. The objective of the paper is to design, stabilize, simulate and implement an autonomous model of a small hovercraft that can travel over any terrains. A real time layered fuzzy navigator for a hovercraft in a dynamic environment is proposed. The system consists of a Takagi-Sugeno-type fuzzy motion planner and a modified proportional navigation based fuzzy controller. The system philosophy is inspired by human routing when moving between obstacles based on visual information including the right and left views from which he makes his next step towards the goal in the free space. It intelligently combines two behaviours to cope with obstacle avoidance as well as approaching a goal using a proportional navigation path accounting for hovercraft kinematics. State-space method is used to represent the dynamics of a hovercraft. MATLAB/Simulink software tool is used to design and verify the proposed algorithm. A practical approach in stabilizing a hovercraft controlled by a fuzzy system based on adaptive nonlinear feedback is presented. This is done using a fuzzy stabilizer in the feedback path of the system. The fuzzy stabilizer is tuned such that its nonlinearity lies in a bounded sector results using the circle criterion theory. An application example for the proposed system has been suggested.

1. INTRODUCTION

Due to their amphibian qualities, hovercrafts are the means of choice if it comes to mobility and transportation in various inaccessible areas. Their biggest advantage, however, which is being almost fully detached from the ground, comes at the cost of reduced and difficult maneuverability. All steering and stopping maneuvers are facilitated through the air thrust generated by the propulsion system [1].

A hovercraft is propelled by an air propeller and support by a skirt or called as cushion of air retained within a flexible structure. The air inside the cushion is retained by a lift fan, which means the fan will absorb the air from the environment and compress into the air cushion. The hovercraft uses rudder mechanism to steer; therefore the fan must produce the sufficient air speed for the rudder to be effective as a control surface [2].

In fact there are different types of hovercraft; one of them is an amphibious hovercraft. The proposed model hovercraft is also supposed to be an amphibious hovercraft, this means it can operate over land and over water.

In the hovercraft; are placed two propellers both driven by an electric motor and one of them is used to provide lift by keeping a low-pressure air cavity under the craft full of air. As the air pressure is increased the air lifts the craft by filling the cavity. The cavity or chamber in which the air is kept is called a 'plenum' chamber. At the point when the air pressure equals the weight of the hovercraft over the chambers surface area the hovercraft lifts and the air starts to escape through two holes made in the bottom plate. The escaped air creates an air-lubricated layer between the hovercraft and the ground surface. This will lead to a frictionless motion of the hovercraft, taken into account that the minimum contact between skirt and the ground surface during the motion is negligible. The amount of the total weight that a hovercraft can raise is equal to the pressure in the plenum chamber multiplied by the area of the hovercraft. In basic hovercrafts does the air escape around the edge of the skirt, but the main principle is the same. This plenum chamber principle is visualized in Fig.1.

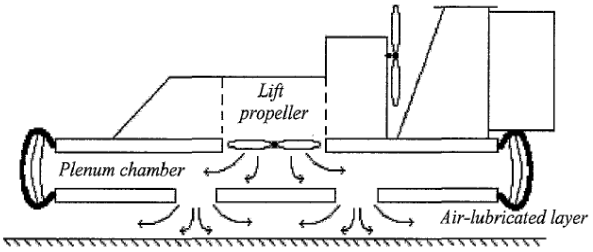

Fig.1 Twin engine Hovercraft

A constant feed of air is needed to lift the hovercraft and to compensate for the air being lost through the holes in the bottom plate. The flow must also be greater than the amount of air that escapes through the holes in the bottom plate. The rate of the air loss is not constant, because there is no way of ensuring that any air escapes evenly all around the hovercraft. To maintain also the lift, the engine and propeller have to be sufficiently powerful enough to provide a high airflow rate into the chamber.

A cylinder is placed around the lift propeller to improve the efficiency, because it reduces the pressure loss around the propeller tube.

The second propeller is driven by another motor and is placed on the back end of the hovercraft. This motor can only deliver a constant speed to the propeller in contrast to the lift propeller and is used to generate a displacement forward. The propeller can deliver a maximum force of 1,8 N, when there is no wind and the battery is fully charged. This model hovercraft can reach a maximum speed of 3 m/s when full lift is generated and if the rudder is in default position so that the hovercraft only moves in a straight line.

Without a rudder the hovercraft is unmanoeuvrable. Therefore a vertical rudder is placed on the back of the hovercraft behind the back thrust propeller. Conventional hovercrafts normally have a very high rudder position over the center of gravity. Its action not only creates turning moments but also a drifting force and rolling moment, which leads to an outward-banked turn.

2. HOVERCRAFT STRUCTURE AND DESIGN

The structure of a model Hovercraft should be both light and strong. In addition, if a model is to operate over water it must be water resistant and buoyant [3]. Since the RC Hovercraft must be lightweight they have more in common with RC Aircraft than boats. Traditional Aircraft modeling methods use balsa construction. This result in a light and strong model, but this type of construction is very difficult to be water proof. In addition it is not very robust and inevitable knocks and scrapes are often sustained by model as it operates encounters obstacles. Other materials such as styrene and plywood sheet are obtainable in a variety of gauges and more robust but still very light. Modern high impact styrene sheets have become poplar and can be found in many models stores. In addition, the size of the model which must be convenient size to be easy carried and stored in the lab. Also, the mass of the model plays an important role in its design, it must be light to provide easier control and to use less power motor and give longer life battery.

2.1 Hovercraft Computer Aided Design (CAD) Model

CAD model is drawn using Solid Edge^{TM} V20, and Fig.2 showing each part of the assembly drawing.

a. The Hull

The hull of the hovercraft consists of a low density balsa construction, with dimensions of 750mm*500mm*50mm, and wall thickness is 6 mm. The main forces that affect the hovercraft are the forces and moments exerted by the propulsion unit, the aerodynamic forces and moments exerted by the airflow (most notably, the drag) and finally the weight force.

b. The Rotor Propellers

The propellers used in the physical model are ready made ones, therefore the model is not very accurate, the main forces of propeller are Rotation around the axis of the rotor, this is the main and most obvious motion, the aerodynamic forces and moments exerted by the airflow and finally the weight forces of the propeller which we neglected in our model because it weighs less than 7 grams.

c. The motor

Hovercraft model has two DC brushless servo motor one for lift (hovering) the craft and the other for supporting the thrust force to the craft to move forward.

This motor will hold the propeller. Together the DC motor and the propeller will be our propulsion unit and there was no need to a hub or a simple gear box since we are using a high torque generating motors compared to its size.

d. The Mount:

It is a casing contains the propeller for safety reasons, and to make the air ducted in one direction to avoid wasting motor output power.

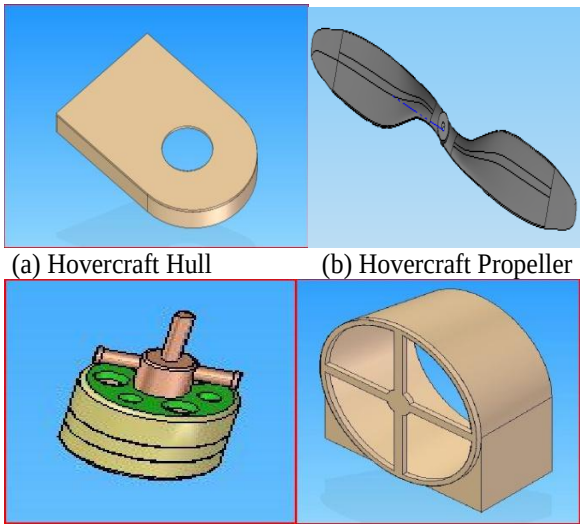

(a) Hovercraft Hull (b) Hovercraft Propeller

(c) Hovercraft motor (d) Hovercraft mount

Fig.2 The parts of the assembly drawing.

e. ASSEMBLY DRAWING

The battery and electronic circuits will be acting by weight forces only. Figure 3 shows the assembly of the model and the main axes of direction are considered the positive direction while studying the Simulink model of the hovercraft.

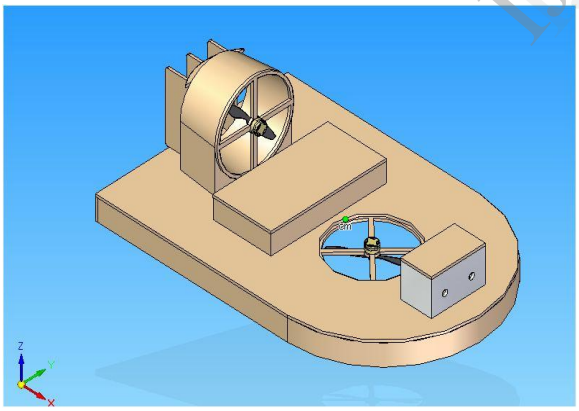

Fig.3 Hovercraft assembly drawing

f. Mass and inertial properties

Mass properties

These properties were estimated using the inspection tool of Solid edge, the mass properties of each part is illustrated on table 1

Table 1 Mass properties

Item	Mass (grams)	Quantity	Total mass
battery	147	2	294
Control circuits	225	1	225
DC motor	39	2	78
ESC	15	2	30
receiver	40	1	40
propeller	7	2	14

Inertial properties

These properties were estimated using the inspection tool of Solid edge to be used in the Simulink model parameters, the inertial properties of each part is illustrated on Table 2

Table 2 Inertial properties

Axis	M.M. Inertia	Radii of Gyration
X	0.098562 kg-m^2	240.333073 mm
Y	0.085518 kg-m^2	223.866049 mm
Z	0.016975 kg-m^2	99.738627 mm

2.2 Hovercraft Equations of motion

The derivation of equations of motion, the first and most essential step in developing the hovercraft mathematical model, represents the hovercraft movement on a two dimensional plane. The hovercraft has two fans one thrust fan and one lift fan. The thrust fan provided single input F. Figure 4 depicts hovercraft location and orientation (x,y,θ) along with the sites of possible applied force.

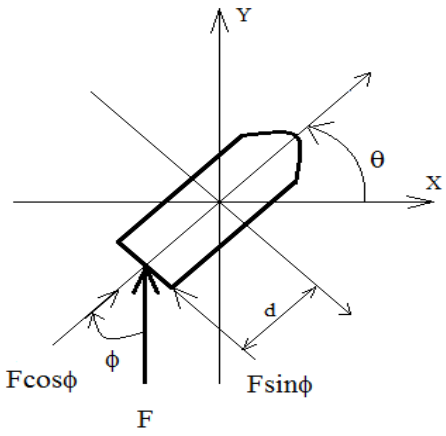

Fig.4. Forces Analysis on Hovercraft

The force analysis was possible with derivation from Newton's second law .

$$\sum \mathbf{F} = \mathbf{M} \times \mathbf{A} \qquad (1)$$

where:

F is the applied force

M is the object mass

A the object acceleration

a. The analysis in the X-direction

The hovercraft frame axis has an angle with the applied force F which can be analyze along the frame axes. Then, using Newton's second law, the acceleration component along the X- axis can be calculated as followed:

$$\mathbf{F}\cos\varphi\cos\theta + \mathbf{F}\sin\varphi\cos\theta = \mathbf{M} \times \ddot{\mathbf{X}} \qquad (2)$$

$$\ddot{\mathbf{X}} = \frac{\mathbf{F}\cos\varphi\cos\theta + \mathbf{F}\sin\varphi\cos\theta}{\mathbf{M}}$$

The analysis in the Y direction

$$\mathbf{F}\cos\varphi\sin\theta - \mathbf{F}\sin\varphi\sin\theta = \mathbf{M} \times \ddot{\mathbf{Y}} \qquad (3)$$

$$\ddot{\mathbf{Y}} = \frac{\mathbf{F}\cos\varphi\sin\theta - \mathbf{F}\sin\varphi\sin\theta}{\mathbf{M}}$$

The analysis of Rotational motion

Equating the following equation to Newton's 2^{nd} law in terms of rotational motion, where **I** is the moment of inertia, and is $\ddot{\theta}$ the angular acceleration as follows:

$$\sum \mathbf{T} = \mathbf{I} \times \boldsymbol{\alpha} = \mathbf{I} \times \ddot{\boldsymbol{\theta}} \qquad (4)$$

Consider the perpendicular distance **d** (the distance between the applied force and the center of the hovercraft) with the applied force which act as the torque applied on the hovercraft:

$$\mathbf{I} \times \ddot{\boldsymbol{\theta}} = \mathbf{F}\sin\varphi \times \mathbf{d}$$

$$\ddot{\boldsymbol{\theta}} = \frac{\mathbf{F}\sin\varphi \times \mathbf{d}}{\mathbf{I}} \qquad (5)$$

b. The equation of motion with Friction

Because the hovercraft rides on a cushion of air and has little contact with the ground, only viscous friction (fluid friction or in this case ground resistance) was considered. Including the hovercraft had a viscous friction in the opposite direction to the hovercraft's motion represented by F_f. The friction force is defined by:

$$\mathbf{F_f} = \mathbf{b} \times \mathbf{N} = \mathbf{b} \times \mathbf{m} \times \mathbf{g} \qquad (6)$$

Where:

b is the coefficient of friction.

N is the difference between hovercraft's weight and lift force.

m is the hovercraft's mass.

g is specific gravity.

The analysis in the X-direction

The viscous force is proportional to the hovercraft's velocity, giving the relationship

$$F_f = -bu$$

$$\mathbf{F}\cos\varphi\cos\theta + \mathbf{F}\sin\varphi\cos\theta - \mathbf{bu} = \mathbf{m} \times \dot{\mathbf{u}}$$

$$\dot{\mathbf{u}} = \frac{\mathbf{F}\cos\varphi\cos\theta + \mathbf{F}\sin\varphi\cos\theta - \mathbf{bu}}{\mathbf{m}} \qquad (7)$$

The analysis in the Y direction

$$\mathbf{F}\cos\varphi\sin\theta - \mathbf{F}\sin\varphi\sin\theta - \mathbf{bv} = \mathbf{m} \times \dot{\mathbf{v}}$$

$$\dot{\mathbf{v}} = \frac{\mathbf{F}\cos\varphi\sin\theta - \mathbf{F}\sin\varphi\sin\theta - \mathbf{bv}}{\mathbf{m}} \qquad (8)$$

c. The analysis of rotational motion

Equating the following equation to Newton's 2^{nd} law in terms of rotational motion where Iis the moment of inertia, and $\dot{\omega}$ is the angular acceleration, the rotational coefficient of viscous frictionb_θ is said to relate viscous torque to angular velocity, then we calculate the angular acceleration from the difference between the component of the applied torque and rotational viscous friction as follows:

$$dF\sin\varphi = I\,\dot{\omega}$$

$$\dot{\omega} = \frac{dF\sin\varphi - b_\theta \omega}{I} \tag{9}$$

d. Defining modelling parameters

The viscous translational coefficient of friction was estimated with an experiment governed by the differential equation:

$$m\ddot{x} = -b\,\dot{x}$$

$$\dot{x} = v$$

$\dot{v} + \frac{bv}{m} = 0$, let $v = e^{\lambda t}$ then $\dot{v} = e^{\lambda t}$, substitute in the previous equation we get:

$\lambda e^{\lambda t} + \frac{b}{m} e^{\lambda t} = 0$, then $\lambda = -\frac{b}{m}$, then the solution is

$$v = v_\circ e^{-\frac{bt}{m}}$$

while rotational motion was governed by:

$$I\ddot{\theta} = -b_\theta \dot{\theta}$$

$$\dot{\theta} = \omega$$

$\dot{\omega} + \frac{b_\theta \omega}{I} = 0$, let $\omega = e^{\lambda t}$ then $\dot{\omega} = e^{\lambda t}$, substitute in the previous equation we get: $\lambda e^{\lambda t} + \frac{b_\theta}{I} e^{\lambda t} = 0$ then

$$\lambda = -\frac{b_\theta}{I}$$

With a final velocity (v) equal to zero, velocity descends exponentially from max towards zero over time. By substituting $5\,\tau$ for time to stop (τ in this case equal $m \setminus b$), it can be solved for the translational viscous coefficient $b \approx \frac{5\,m}{T_{stop}}$.

By bringing the hovercraft to a determined top speed in a straight line and allowing it to stop, T_{stop} can be measured and b can be estimated.

The subsequent Fig.5, plots $v = v_\circ e^{-\frac{bt}{m}}$ for the hovercraft. Choosing 5τ to represent stopping time proved to be reasonable, the stopping time experimentally was 15 seconds , a point at which the plot shows a velocity close to zero ,the mass of hovercraft which calculated from the sum of each component's weight was 0.681kg. By substituting, the measured translational viscous coefficient was 0.227 kg/sec.

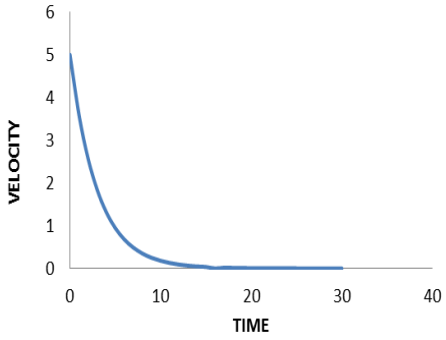

Fig.5.The velocity - Time curve

Determining the rotational coefficient of viscous friction was accomplished with a very similar method except that instead of the hovercraft beginning with a maximum translational velocity, it begins the experiment with its greatest rotational velocity according to the Fig .6,

$$b_\theta \approx \frac{5\,I}{T_{stop}}$$

.The moment of inertia was estimated by using the inspection tool of the solid edge in the rotational axes x, y, z were respectively ($0.098562 kg.m^2$,0.085518 $kg.m^2$, 0.016975 $kg.m^2$), and we take the value of the moment of inertia in the z axis which is the rotational one , the stopping time experimentally was 20 second. A point at which the plot shows a angular velocity close to zero, then the measured rotational viscous coefficient was 0.004 $kg.kg.m^2/sec$.

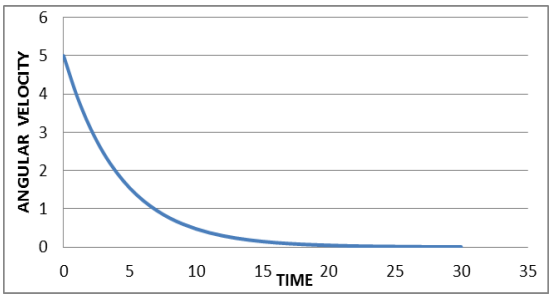

Fig.6.The Angular Velocity - Time curve

2.3 State Space Modeling

State-space models represent the dynamics of physical systems described by a series of first order coupled differential equations. In the general state-

space model, x $\in R^n$ is the state vector and y is the output. The set of equations is given by:

$$\dot{x} = Ax + Bu$$

$$y = Cx + Du$$

The column vector 'x' is called the state of the system. The state of the system is a set of variables describe the future response of a system, given the present state, the excitation inputs and the equations describing the dynamics. For mechanical systems, the state vector elements usually consist of the positions and velocities of the separate bodies, as a result let:

$$\dot{x} = u \quad (10)$$

$$\dot{y} = v \quad (11)$$

$$\dot{\theta} = \omega \quad (12)$$

$$\dot{u} = \frac{F\cos\varphi\cos\theta - F\sin\varphi\sin\theta - bu}{m} \quad (13)$$

$$\dot{v} = \frac{F\cos\varphi\sin\theta + F\sin\varphi\cos\theta - bv}{m} \quad (14)$$

$$\dot{\omega} = \frac{dF\sin\varphi - b_\theta\omega}{I} \quad (15)$$

The values of the rows and columns of the matrix are calculated from the previous equations described the velocity and we take the second part of the equations which described the effect of the viscous friction on the system and we make some assumptions for the linearization for the system that made the value of the angle of the system is so small and near to be equal zero ($\theta \approx 0$) as in Fig.7 , the value of ($\cos\theta = 1$) and the value of ($\sin\theta = 0$),then the equations are:

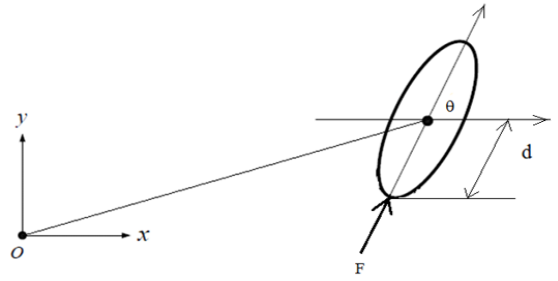

Fig.7. Forces analysis (friction case)

Let $Fx = F\cos\phi$

$Fy = F\sin\phi$

$$\dot{u} = \frac{Fx - bu}{m} \quad (16)$$

$$\dot{v} = \frac{Fy - bv}{m} \quad (17)$$

$$\dot{\omega} = \frac{Fy \cdot d - b_\theta\omega}{I} \quad (18)$$

Then the equations in the state space representation form can be written as follows:

$$\begin{bmatrix}\dot{x}\\ \dot{y}\\ \dot{\theta}\\ \dot{u}\\ \dot{v}\\ \dot{\omega}\end{bmatrix} = \begin{bmatrix}0&0&0&1&0&0\\ 0&0&0&0&1&0\\ 0&0&0&0&0&1\\ 0&0&0&-\frac{b}{m}&0&0\\ 0&0&0&0&-\frac{b}{m}&0\\ 0&0&0&0&0&-\frac{b_\theta}{I}\end{bmatrix}\begin{bmatrix}x\\ y\\ \theta\\ u\\ v\\ \omega\end{bmatrix} + \begin{bmatrix}0&0\\ 0&0\\ 0&0\\ \frac{1}{m}&0\\ 0&\frac{1}{m}\\ 0&\frac{d}{I}\end{bmatrix}\begin{bmatrix}Fx\\ Fy\end{bmatrix} \quad (19)$$

$$C = [1 \quad 1 \quad 10 \quad 0 \quad 0] \quad (20)$$

$$D = [0\ 0] \quad (21)$$

The previous state space representation shows the relations between the position of the hovercraft and its velocity with the effect of the input force. It acts on the rudder to guide the hovercraft in the active motion and its turning to right and left. While nyquist is a graphical technique, it only provides a limited amount of intuition for why a system is stable or unstable, or how to modify an unstable system to be stable as shown in Fig .8.

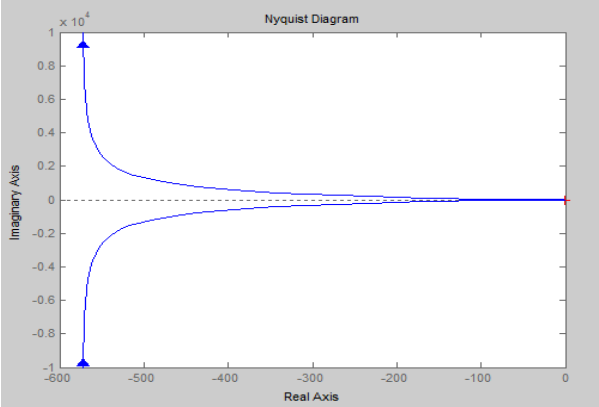

Fig.8. Nyquist plot of the system

2.4 Hovercraft Simulink Model

The simulation of the power system is an important means to study the dynamic performance of the power system of hovercrafts. The simulation model is established based on matlab/simulink with the method of system simulation. Through selecting of typical operating conditions and setting of parameters the simulation model and program are checked and debugged and then the simulation calculations of dynamic performance under typical conditions are made.

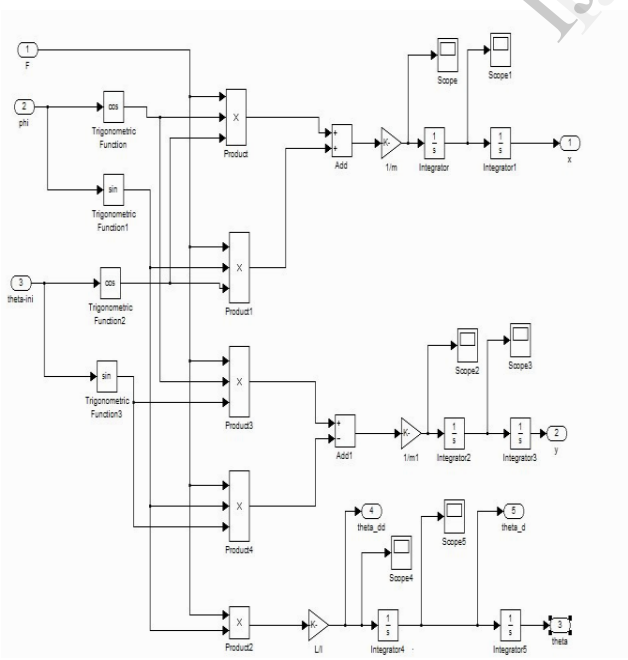

Fig.9. System dynamics subsystems

3. FUZZY LOGIC IN AUTONOMOUS NAVIGATION

A number of different strategies has been published in the use of fuzzy logic in autonomous navigation[4]. The use of fuzzy logic in mobile robotics was reported in 1985 by Sugeno and Nishida [5] who developed a fuzzy controller capable of driving a model car along a track delimited by two walls. In 1988, Tekeucho et al [6] published a simple fuzzy logic based obstacle avoidance algorithm. The behavioural based structure has been used in [7-9], in which different behaviours are assigned for different situations. However, the increased level of behaviours employed is accompanied by an increase in complexity of the resulting system. As the number of system variables increases, the number of rules in the conventional complete rule set increases exponentially.

The concept of "hierarchical structure" is used [10, 11] to tackle the problem wherein the number of rules increase linearly (not exponentially) with the number of the system variable. Unfortunately, the structure needs more training and additional algorithms for tuning the fuzzy parameters. All the behaviours suggested can be considered as simple, in that they only take into account one single objective. However, to perform autonomous navigation, the vehicle should be able to perform complex tasks that take multiple objectives into account; for example, going to a goal while avoiding unforeseen obstacles in real time.

Fuzzy controllers are typically designed to consider one single goal [12]. If we want to consider several interacting goals, we have two options. We can write different sets of simpler rules, one specific to each goal, and combine their outputs in some way. This will increase the hardware requirements of the system. Alternatively we can write one set of complex rules whose antecedents consider both goals simultaneously. Defining rules for such a system leads to more efficient hardware implementation [13]. This paper focuses on the design of a fuzzy navigator for real time motion in a dynamic environment based on a complex rule base inspired by human capabilities.

3.1 Design and Simulation of the Layered Fuzzy Navigator

Intelligent vehicle systems should take task-level commands directly without any planning-type decomposition [14, 15]. Additionally it is desirable to design them for a large class of tasks rather than a specific task. As a result, the spilt between vehicle controller design and vehicle action planning is critical since they usually have two different reference bases. The action planning is carried out in terms of events, whereas the execution of planned actions uses a reference frame on existing vehicle control system using a time based or clocked trajectory. The presented system consists of two subsystems, a fuzzy motion planner (FMP) and a modified proportional navigation (PN) based fuzzy controller as illustrated in Fig.10.

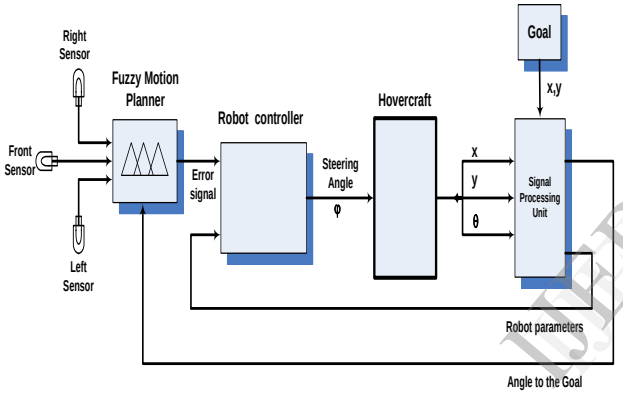

Fig.10 The complete system of fuzzy motion planner and behavioural fuzzy controller

The data from the three sensors plus the direction to the goal are input to the motion planner resulting is a clear direction to move in. Next, the fuzzy controller decides the direction to steer the hovercraft to the goal using the proportional navigation trajectory avoiding the obstacles. The signal processing unit is responsible for calculating the line of sight rate of change and the required steering angle to the goal

The system philosophy is inspired by human routing when moving between obstacles based on visual information including right and left views to identify the next step to the goal in obstacle-free space [16]. This is analogous to the proposed vehicle moving safely in an environment based on data "visible" with three ultrasound range finders. These sensors are mounted to the front, right and left of the hovercraft as shown in Fig.11.

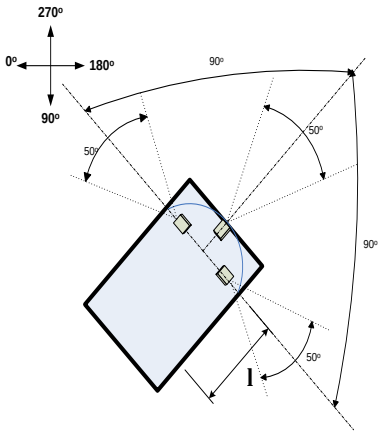

Fig.11 The Robot Sensors with their beam pattern

The sensors are modelled such that they scan an array of zeros representing the clear environment with obstacles set to ones if present. They scan the array in a 50^{o} sector along each sensor axis direction such that it returns the range of the nearest obstacle as shown in Fig.11. The maximum range is set to 5 meters. These specifications meet commercial sensors specifications such as Ultrasonic range finder SRF04, SRF05 and SRF10 [6].

A Sugeno-type [17], fuzzy motion planner of four inputs one output is introduced to give an obstacle-free direction to the vehicle controller. The inputs are the frontal, right and left obstacle ranges found by the front, right and left sensors. The last input is the angle to the goal, which indicates the difference in direction between the goal and the vehicle's current direction. The output is an error angle representing the angle needed to go from the vehicle's direction to a free (suggested) direction. Fuzzy membership functions are assigned to each input as shown in Fig.12.

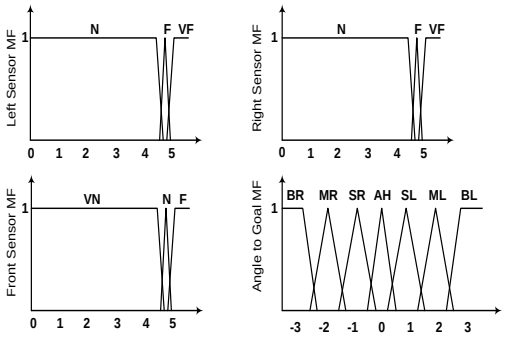

Fig.12 The Membership functions of the fuzzy motion planner inputs

The membership functions describe the ranges from

MF Name	Type	Value	Description
SL	Const.	0.523	Small to the left (30o)
BL	Const.	0.785	Big to the left (45o)
SR	Const.	-0.523	Small to the right(30o)
BR	Const.	-0.785	Big to the right (45o)
F	Const.	0	Forward (no change)
GO AL	Linear	4^{th} input	The same angle to the goal as the 4th input

the sensors designed to give the planner early warning. The left and right sensors assign the obstacle as N (near) or VN (very near) for the front sensor if its range approaches 90% of the sensor maximum range. For example: the obstacle is near if its range is about 4.5 meter as the sensor maximum range is 5 meter. This enables the planner to determine the feasible trajectory at an early stage to avoid cul-de-sacs.

The fuzzy motion planner uses Takagi-Sugeno fuzzy inference for the rule evaluation [14, 17]. Unlike other fuzzy control methods [18], the Takagi-Sugeno results in the output of a control function for the system depending on the values of the inputs which is ideal for acting as an interpolation supervisor of multiple linear controllers that are to be applied, respectively, to different operating conditions of a dynamic nonlinear system as in the present case. The output of the planner is the angle to an obstacle-free direction. This goes to the second stage to control the robot direction, described by five membership function as shown in table 3

In order to optimize the membership function width the Whole Overlap, *WO*, index is calculated from the following equation [12]:

$$WO = \frac{\int_x \min(\mu_1(x), \mu_2(x))}{\int_x \max(\mu_1(x), \mu_2(x))}$$

where: $\mu_1(x)$ and $\mu_2(x)$ are two adjacent membership functions.

A low *WO* (about 14%) improves the steady state error and response time [12]. Similarly, the LOS changing rate is fuzzified by seven membership functions. The rules were formulated one-by-one according to the flow chart Fig.13, and then the whole rules-set was analyzed to make it:-

- Complete: any combination of the inputs fired at least one rule.
- Consistent: contains no contradictions.
- Continuous: has no neighbouring rules with output fuzzy sets that have an empty intersection

Table 3 The fuzzy membership function for the output of the Sugeno-type fuzzy motion planner

Notice that the rules are processed in parallel. The system was modelled and simulated using Simulink™, for a given data set of random environments. Different environments with different obstacle distributions are used to test the system performance as shown in Fig.14. The simulation reveals that the system gives good results for non-complicated environments; for example when there is a limited number of obstacles. This is predictable because of the vehicle's kinematics constraints and constant speed's manoeuvre limitation.

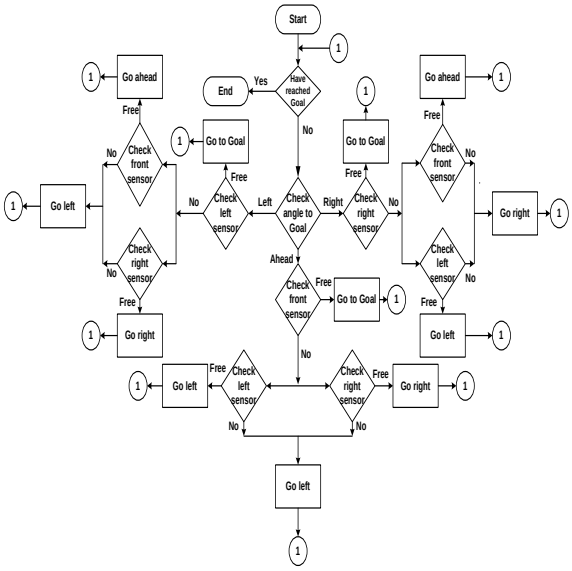

Fig.13 Flow chart of the proposed planner

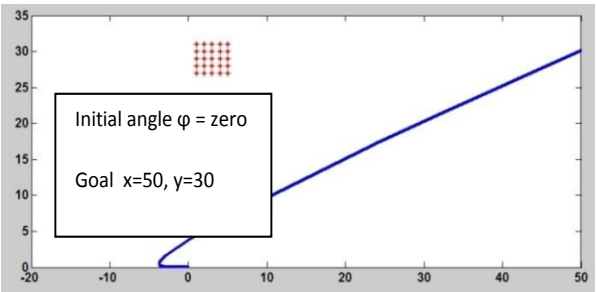

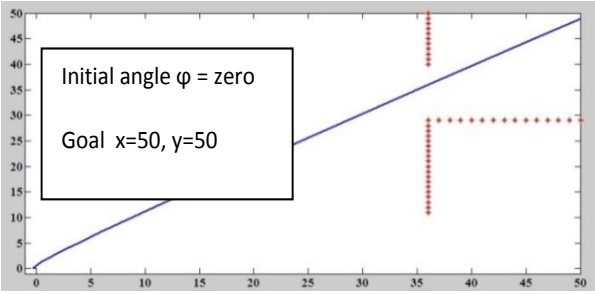

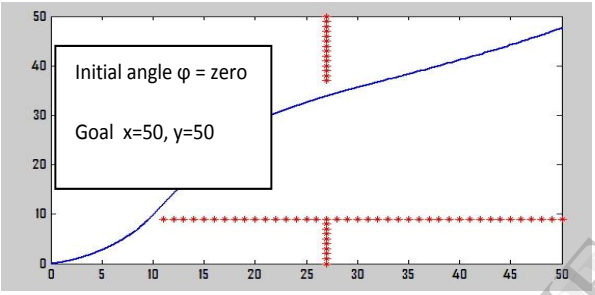

Fig.14 The simulation results for different environments with various obstacle distributions

a. System description

This section concentrates on the ability of stabilizing a closed loop nonlinear proposed system using a Takagi-Sugeno (T-S) fuzzy controller. Fuzzy control based on Takagi-Sugeno (T-S) fuzzy model [19], [18] has been used widely to control nonlinear systems because it efficiently represents a nonlinear system with a set of linear subsystems. The main feature of the T-S fuzzy model is that the consequents of the fuzzy rules are expressed as analytic functions. The choice of the function depends on its practical applications. Specifically, the T–S fuzzy model can be utilized to describe a complex or nonlinear system that cannot be exactly modelled mathematically; the T–S fuzzy model is an interpolation method. The physical complex system is assumed to exhibit explicit linear or nonlinear dynamics around some operating points. These local models are smoothly aggregated via fuzzy inferences, which lead to the construction of complete system dynamics.

Takagi-Sugeno (T-S) fuzzy controller is used in the feedback path as shown in Fig.15, so that it can change the amount of feedback in order to enhance the system performance and its stability [20].

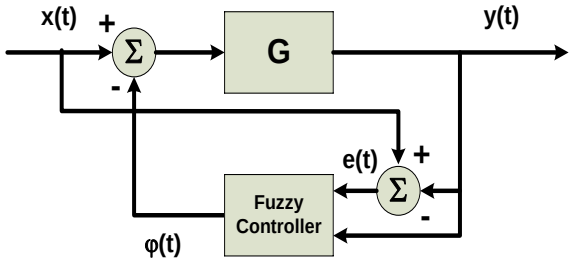

Fig.15 The proposed System block diagram

The proposed fuzzy controller is a two-input one-output system: the error e(t) and open loop output y(t) are the controller inputs while the output is the feedback signal φ(t). The fuzzy controller uses symmetric, normal and uniformly distributed membership functions for the rule premises as shown in Fig. 16(a) and 16(b). Labels have been assigned to every membership function such as NBig (Negative Big) and PBig (Positive Big) etc. Notice that the widths of the membership functions of the input are parameterized by L and h which limited by the physical limitations of the controlled system.

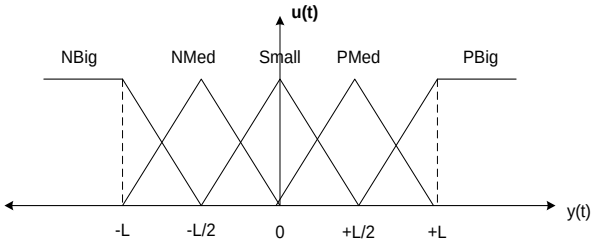

Fig.16(a) The membership distribution of the 2nd input,*y(t)*

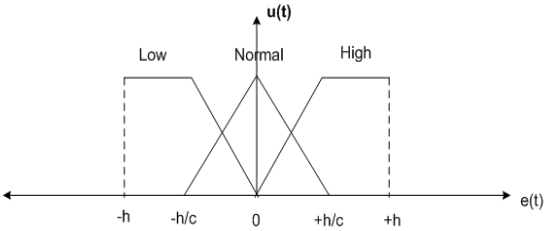

Fig.16(b) The membership distribution of the 1st input, the error *e(t)*

While using the T-S fuzzy model [18], the consequents of the fuzzy rules are expressed as analytic functions which linearly dependent on the inputs. In

our case, three singleton fuzzy terms are assigned to the output such that the consequent φ_c is a linear function of one input $y(t)$ as we can generally write:

$$\varphi_c = r\,M\,y(t) \tag{22}$$

where r takes the values -1, 0, 1

(depends on the output's fuzzy terms)

$y(t)$ is the 2nd input to the controller

M is a parameter used to tune the controller.

The fuzzy rules were formulated such that the output is a feedback signal inversely proportional to the error signal as follow:

IF the error is High THEN $\varphi_c = M\,y(t)$

IF the error is Normal THEN $\varphi_c = 0$

IF the error is Low THEN $\varphi_c = -M\,y(t)$

The fuzzy controller is adjusted by changing the values of L, h and M which affect the controller nonlinearity map. Therefore, the fuzzy controller implemented as these values equivalent to the saturation parameters of standard saturation nonlinearity [21].

4. STABILITY ANALYSIS

Before studying the system stability, first a general model of a Sugeno fuzzy controller shown Fig.17 is defined [22], [19], [18]:

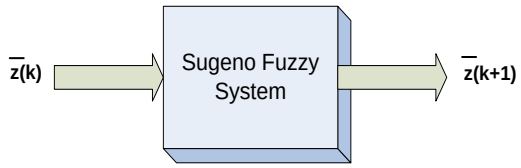

Fig. 17 Block diagram of Sugeno fuzzy system

For a two-input sugeno fuzzy system; let the system state vector at time $t$be:

$$\bar{z}(t) = [z_1(t) \quad z_2(t)]^T$$

where$z_1(t)$, and $z_2(t)$ are the state variable of the system at time t

and a Sugeno fuzzy system is defined by the implications such that:

$$R_i : if \;\; (z_1(t)\ is\ S_1^i \;\; AND \;\; z_2(t)\ is\ S_2^i) \quad then \quad \dot{z}(t) = A_1 z_1(t) + A_2 z_2(t)$$

for $i = 1 \ldots\ldots N$, where

S^i_1 , S^i_2 are the fuzzy set corresponding to the state variables z_1, z_2 and R_i

$A_1, A_2 \in R_{2x2}$, are the characteristic matrices which represent the fuzzy system.

However the truth value of the implication R_i at time t denoted by $w_i(t)$ is defined as:

$$w_i(t) = \wedge(\mu_{S_1^i}(z_1(t)), \mu_{S_2^i}(z_2(t)))$$

where

$\mu_S(z)$ is the membership function value of fuzzy set S at position z

$\wedge$ is taken to be the min operator

Then the system state is updated according to [12]:

$$\dot{z}(t) = \frac{\sum_{i=1}^{N} w_i(t) A_i \bar{z}(t)}{\sum_{i=1}^{N} w_i(t)} = \sum_{i=1}^{N} \delta_i(t) A_i \bar{z}(t) \tag{23}$$

$$\delta_i(t) = \frac{w_i(t)}{\sum_{i=1}^{N} w_i(t)}$$

where

However, the consequent part of the proposed system rules is a linear function of only one input $y(t)$ as mentioned in the previous section, then the output of the fuzzy controller is of the form:

$$\dot{y}(t) = \sum_{i=1}^{N} \delta_i M_i\, y(t) \tag{24}$$

where$N$ is the no. of the rules

M_i is a parameter used for the ith rule to tune the controller

Notice Eq. 24 directly depends on the input y(t) and indirectly depends on $e(t)$ which affects the weights δ_i.

For simplicity of the stability analysis, the proposed system is redrawn as shown in Fig.18

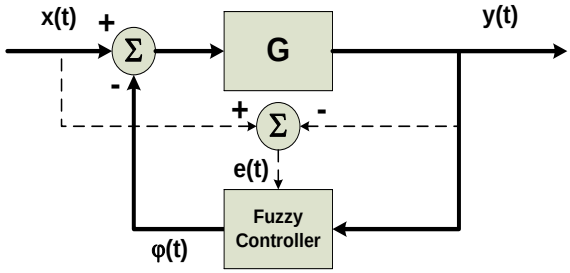

Fig.18 The equivalent block diagram of the proposed system

The stability analysis of the system considers the system nonlinearities and uses circle criterion theory to ensure stability.

4.1 Analysis using Circle Criterion

In this section the circle criterion [21, 23-25] will be used for testing and tuning the controller in order to insure the system stability and improve its output response. The circle criterion was first used in [23, 24] for stability analysis of fuzzy logic controllers and as a result of its graphical nature; the designer is given a physical feel for the system.

Consider a closed loop system, Fig.19, given a linear time-invariant part G (a linear representation of the process to be controlled) with a nonlinear feedback part $\varphi(t)$ (represent a fuzzy controller), that is LUR'E system [23, 24].

As a result a T-S fuzzy system can be represented according to that is, and the nonlinear part expressed by $\varphi(t)$ from Eq.22 which can be rewritten as follow:

$$\dot{y} = \sum_{i=1}^{N} \{M_i y - [(1-\delta_i(y))M_i y]\}$$

Hence the nonlinear part $\varphi(t)$ can be expressed by:

$$\varphi = \sum_{i=1}^{N} [(1-\delta_i(y))M_i y]$$

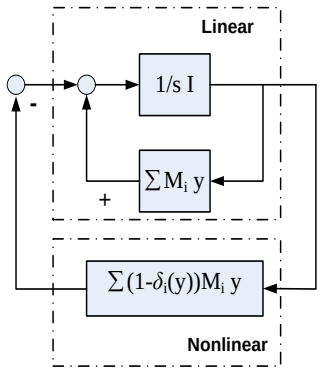

Fig.19 T-S fuzzy system according to the structure of the problem of LUR'E

The function $\varphi(t)$ represents memoryless, time varying nonlinearity with:

$$\varphi : [0,\infty) \times \Re \to \Re$$

If φ is bounded within a certain region as shown in Fig.20 such that there exist:

α, β, a, b, ($\beta > \alpha$, a<0<b) for which:

$$\alpha y \le \varphi(y) \le \beta y \quad (25)$$

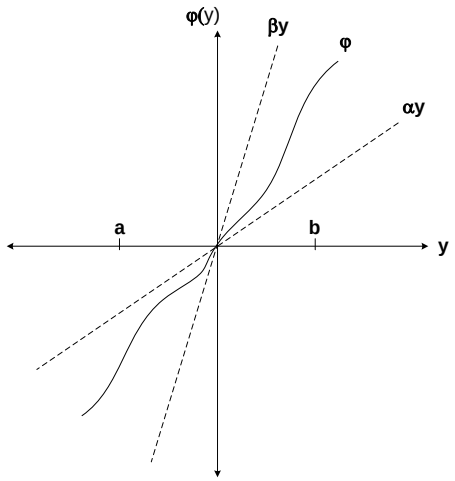

Fig.20 Sector Bounded Nonlinearity

for all $t \ge 0$ and all y ∈ [a, b] then:

$\varphi(y)$is a "Sector Nonlinearity":

If $\alpha y \le \varphi(y) \le \beta y$ is true for all y ∈ (-∞,∞) then the sector condition holds globally and the system is "absolutely stable". The idea is that no detail information about nonlinearity is assumed, all that known it is that φ satisfies this condition [23].

Let D(α, β) denote the closed disk in the complex plane centered at $\frac{(\alpha+\beta)}{2\alpha\beta}$, with radius $\frac{(\alpha-\beta)}{2|\alpha\beta|}$ and the diameter is the line segment connecting the points $\frac{-1}{\alpha}+j0$ and $\frac{-1}{\beta}+j0$.

The circle criterion states that when φ satisfies the sector condition Eq.25 the system in Fig.3 is absolutely stable if one of following conditions is met [23]:

1- If $0 < \alpha < \beta$, the Nyquist Plot of *G(jw)* is bounded away from the disk D(α, β) and encircles it m times in the counter clockwise direction where m is the number of poles of *G(s)* in the open right half plane(RHP).

2- If $0 = \alpha < \beta$, *G(s)* is Hurwitz (poles in the open LHP) and the Nyquist Plot of *G(jw)* lies to the right of the line $s = \frac{-1}{\beta}$.

3- If $\alpha < 0 < \beta$, G(s) is Hurwitz and Nyquist Plot of *G(jw)* lies in the interior of the disk D(α, β) and is bounded away from the circumference of D(α, β).

For the fuzzy controller represented by Eq.22, we are interested in the first two conditions [23], and it can be sector bounded in the same manner [21] such that:

Consider the fuzzy controller as a nonlinearity φ and that there exist a sector (α, β) in which φ lies and use the circle criterion to test the stability. Simply, using the Nyquist plot, the sector bounded nonlinearity of the fuzzy logic controller will degenerate, depending on its slop α that is always zero [21] and the disk to the straight line passing through $\frac{-1}{\beta}$ and parallel to the imaginary axis as shown in Fig.6 In such case the stability criteria will be modified as follows:

Definition: A SISO system will be globally and asymptotically stable provided the complete Nyquist locus of its transfer function does not enter and encircle the forbidden region left to the line passing through $\frac{-1}{\beta}$ in an anticlockwise direction as shown in Fig.21.

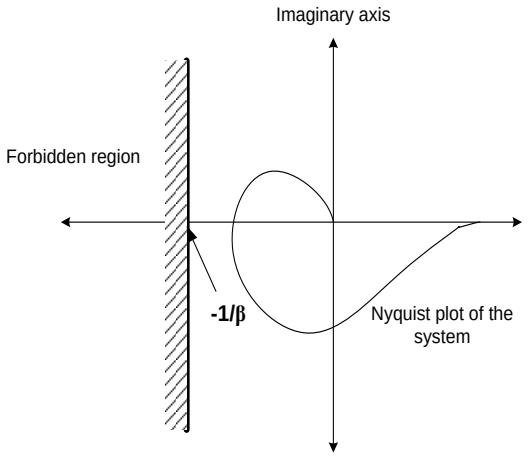

Fig.21 Nyquist plot for fuzzy feedback system [23].

The fuzzy controller is tuned until its parameters lie in the bounded sector. Furthermore the idea can be extended to be used to enhance the performance of an already designed control system especially for the systems controlled using fuzzy controller in the forward loop. For such systems the feedback fuzzy stabilizer can be integrated in the main fuzzy controller as explained in next section.

4.2 Simulation Results

The fuzzy controller is adjusted by changing the values of L, h and *M* which affect the controller nonlinearity map. Therefore, the fuzzy controller implemented as these values equivalent to the saturation parameters of standard saturation nonlinearity. The Nyquist plot of the proposed system was shown before in Fig.8.

If we consider the fuzzy stabilizer as a nonlinearity φ as shown in Fig 6, then the disk D(α, β) is the line segment connecting the points $\frac{-1}{\alpha}+j0$ and $\frac{-1}{\beta}+j0$. Applying the Circle Criterion and because $\alpha = 0$ the second condition will be used. To find a sector (α, β) in which φ lies, the system Nyquist plot Fig.8 is analyzed. The Nyquist plot does not satisfy the second condition as it intersects with the line drawn at $\frac{-1}{\beta}$. As a result to meet the second condition of the theory the line drawn at $\frac{-1}{\beta}$ will be moved to be at $\frac{-1}{\beta} = -590$

such that the Nyquist plot lies to the right of it. However, the fuzzy controller will be tuned by choosing M, and L such that its nonlinearities lies in the sector (0, 0.0016).

It is clear that the values of M and L will be limited by the physical limitation of the plant; however the ratio M/L will be kept less than β (i.e M/L < 0.0017). In our proposed system, choose M=0.134 and L= 120.

Simulations to compare results between the system step response (Black curve) with and without the use of the stabilizer (dotted curve) are shown Fig. 22.

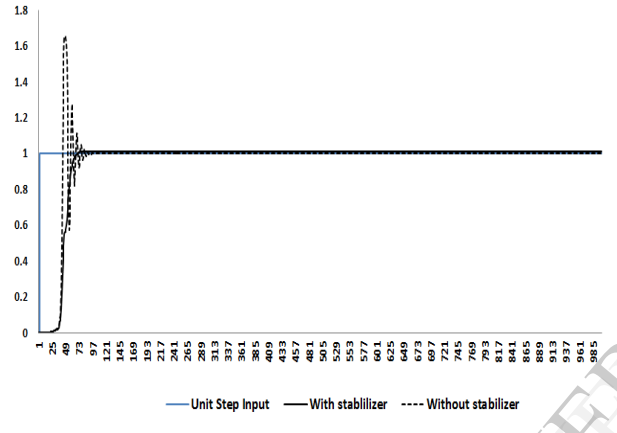

Fig.22 The simulated step response of the two compared systems

4.3 The Proposed hovercraft application example

Today the Hovercraft is used for a variety of civil and military applications. The ability of the craft to cross a variety of terrain as well as being amphibian makes this a very flexible transportation method.

The major value of hovercraft is they can reach areas that are inaccessible on foot or by conventional vehicles and the fact that a hovercraft is above and not in the water is a big advantage in wars zones where the water may be mined. A hovercraft will just glide over a mine without setting it off. As a result, the proposed system can be equipped with mining detection system in order to give early warning about mines see Fig.(23)

Fig (23) The hovercraft equipped with mine detector

5. CONCLUSION

The aim of the present paper was to present a practical approach in stabilizing and design a hovercraft controlled by a fuzzy system based on adaptive nonlinear feedback. This is done using a fuzzy stabilizer in the feedback path of the system. The fuzzy stabilizer is tuned such that its nonlinearity lies in a bounded sector results using the circle criterion theory. Because of circle criterion graphical nature; the designer is given a physical feel for the system

The advantage of the proposed approach is the simplicity of the design procedure. The use of the fuzzy system to control the feedback loop using its approximate reasoning algorithm gives a good opportunity to handle the practical system uncertainty.

A simplified Matlab/Simulink model is considered for good parameter design The obstacle avoidance technique considered for real time motion in a dynamic environment based on a complex rule base and inspired by human capabilities. The system consists of two layers: a Takagi-Sugeno-type fuzzy motion planner; and a modified proportional navigation based fuzzy controller. The system uses Takagi-Sugeno fuzzy inference for the rule evaluation which allows piecewise refinement of a linear relationship of the form that appears in the rule's consequent. The system intelligently combines two behaviours to cope with obstacle avoidance as well goal-approaching using a proportional navigation path accounting for hovercraft kinematics. An application example for the proposed system has been suggested.

REFERENCES

1. Sanders, R.M.W., *Control of a Model Sized Hovercraft*, 2003, The University of New South Wales: Aydney, Australia.
2. Hein, S.M. and H. Choo, *Design and development of a compact hovercraft vehicle*, in *IEEE/ASME International Conference on Advanced Intelligent Mechatronics (AIM), 2013*2013: Wollongong, NSW. p.1516 - 1521.
3. Yun, L. and A. Bliault, *Theory and Design of Air Cushion Craft*2000, New York, NY, USA: John Wiley & Sons Inc.
4. Precup, R.-E. and H. Hellendoorn, *A survey on industrial applications of fuzzy control.* Computers in Industry, 2011. **62**: p. 213-226.
5. Sugeno, M. and M. Nishida, *Fuzzy Control of Model Car.* Fuzzy Sets&Systems, 1985. **16**(2):
6. Takeuchi, T., Y. Nagai, and N. Enomoto, *Fuzzy Control of a Mobile Robot for Obstacle Avoidance.* Information Sciences, 1988. **45**(2):
7. Parasuraman, S., V. Ganapathy, and B. Shirinzadeh, *Behavior based mobile robot navigation by AI techniques: Behavior selection and resolving behavior conflicts using α-level fuzzy inference system*, in *the ICGST International Conference on Automation, Robotics and Autonomous Systems (ARAS-05)*2005: Cairo, Egypt.
8. Vadakkepat, P., et al., *Fuzzy Behavior-Based Control of Mobile Robots.* IEEE Transactions on Fuzzy Systems, 2004. **12**(4): p. 559-564.
9. Seraji, H. and A. Howard, *Behavior-Based Robot Navigation on Challenging Terrain: A Fuzzy Logic Approach.* IEEE Trans. on Robotics And Automation, 2002. **18**(3):
10. Lin., W.S., C.L. Huang, and C.M. K., *Hierarchical Fuzzy Control for Autonomous Navigation of Wheeled Robots.* IEE Proceedings - Control Theory and Applications, 2005. **125**(5): p. 598-606.
11. Hagras, H.A., *A Hierarchical Type-2 Fuzzy Logic Control Architecture for Autonomous Mobile Robots.* IEEE Transactions on Fuzzy Systems, 2004. **12**(4): p. 524-539.
12. Reznik, L., *Fuzzy Contollers*1997: Newnes.
13. Elkhatib, M.M. and W.M. Hussein. *Design, Modelling, Implementation and Intelligent fuzzy control of a Hovercraft*. in *The SPIE Defense, Security, and Sensing conference*. 2011. Orlando, Florida, United States.
14. Olajubu, E.A., at. al., *A fuzzy logic based multi-agents controller.* Expert Systems with Applications, 2011. **38**: p. 4860-4865.
15. Gupta, K. and A.P. Pobil, *Practical Motion Planning in Robotics: Current approach and Future Directions*1998:John Wiley&Sons Ltd.
16. El-Demerdash, A.B., et al. *UAV Mathematical Modeling, Analysis and Fuzzy Controller Design*. in *The 15th International Conference on AEROSPACE SCIENCES & AVIATION TECHNOLOGY*. 2013. MTC, Cairo, EGYPT.
17. Walker, K. and A.C. Esterline. *Fuzzy motion planning using the Takagi-Sugeno method*. in *Proceeding of the IEEE Southeastcon 2000*. 2000. Nashville, TN, USA.
18. Buckley, J.J. and E. Eslami, *An Introduction to Fuzzy Logic and Fuzzy Sets*2002: Phydica-Verlag Heidelberg.
19. Babuska, R., J. Roubos, and H. Verbruggen, *Identification of MIMO systems by input-output TS fuzzy models*, in *In the proceedings of The 1998 IEEE International Conference on Fuzzy systems, IEEE World Congress on Computational Intelligence*1998.
20. Elkhatib, M.M. and J.J. Soraghan, *Fuzzy stabilization of fuzzy control systems*, in *New Approaches in Automation and Robotics*, H. Aschemann, Editor 2008, I-Tech Education and Publishing: Vienna, Austria, EU.
21. Jenkins, D. and K.M. Passino, *An Introduction to Nonlinear Analysis of Fuzzy Control Systems.* Journal of Intelligent and Fuzzy Systems,, 1999. **17**(1): p. 75–103.
22. Thathachar, M.A.L. and P. Viswanath, *On the stability of fuzzy systems.* IEEE Transaction on Fuzzy Systems, 1997. **5**(1): p. 145-151.
23. Ray, K.S., A.M. Ghosh, and D.D. Majumder, *L2-Stability and the related design concept for SISO linear systems associated with fuzzy logic controllers.* IEEE Transactions on Sys., Man & Cyber., 1984. **SMC-14**(6): p. 932–939.
24. Ray, K.S. and D.D. Majumderr, *Application of circle criteria for stability analysis of linear SISO and MIMO systems associated with fuzzy logic controllers.* IEEE Transactions on Systems, Man, and Cybernetics, 1984. **SMC-14**(2): p. 345–349.
25. Vidyasagar, M., *Nonlinear Systems Analysis*1993, Englewood, Cliffs, New Jersey: Prentice Hall, Inc.